Inorg. Chem. **2007**, *46*, 9779–9789

$[Os(bipy)(CN)_4]^{2-}$ and Its Relatives as Components of Polynuclear Assemblies: Structural and Photophysical Properties

Svetlana G. Baca, Harry Adams, Christopher S. Grange, Alec P. Smith, Igor Sazanovich, and Michael D. Ward*

Department of Chemistry, University of Sheffield, Sheffield, S3 7HF, UK

Received June 15, 2007

A series of diimine-tetracyanoosmate anions $[Os(diimine)(CN)_4]^{2-}$ [diimine = 2,2′-bipyridine (bipy), 2,2′-bipyrimidine (bpym), 1,10-phenanthroline (phen), and 4,4′-^{t}Bu$_2$-2,2′-bipyridine (^{t}Bu$_2$bpy)] were prepared and isolated as their Na^+ salts (water soluble) or PPN^+ salts (soluble in organic solvents). Several examples were crystallographically characterized; the Na^+ salts form a range of 1D, 2D, or 3D infinite coordination polymers via coordination of the cyanide groups to Na^+ cations in either an end-on or a side-on manner. The $[Os(diimine)(CN)_4]^{2-}$ anions are solvatochromic, showing three MLCT absorptions, which are considerably blue-shifted in water compared to organic solvents, in the same way as is well-known for the analogous $[Ru(diimine)(CN)_4]^{2-}$ anions. Luminescence in the red region of the spectrum is very weak but (following the expected solvatochromic behavior) is higher energy and more intense in water. However, by exploiting the effect of metallochromism (ref 4), the emission from $[Os(^t Bu_2bpy)(CN)_4]^{2-}$ in MeCN can be very substantially boosted in energy, intensity, and lifetime in the presence of Lewis-acidic metal cations (Na^+, Ba^{2+}, Zn^{2+}), which, in a relatively noncompetitive solvent, coordinate to the cyanide groups of $[Os(^t Bu_2bpy)(CN)_4]^{2-}$. This has an effect similar in principle to hydrogen bonding of the cyanides to $\delta+$ protons of water, but very much stronger, such that in the presence of Zn^{2+} ions in MeCN the ^{1}MLCT and ^{3}MLCT absorptions are blue-shifted by ca. 7000 cm^{-1}, and the luminescence moves from 970 nm (vanishingly weak) to 610 nm with a lifetime of 120 ns (dominant component). Thus, the binding of metal cations to the cyanides provides a mechanism to incorporate $[Os(diimine)(CN)_4]^{2-}$ complexes into polynuclear assemblies and simultaneously increases their ^{3}MLCT energy and lifetime to an extent that makes them comparable to much-stronger luminophores such as Ru(II)-polypyridines.

Introduction

In recent years, we and others have started to exploit the deceptively simple complex $[Ru(bipy)(CN)_4]^{2-}$ as a component of supramolecular assemblies that display useful photophysical properties.[1] Compared to the much-better-known complex $[Ru(bipy)_3]^{2+}$, $[Ru(bipy)(CN)_4]^{2-}$ offers numerous significant advantages, which may be summarized as follows: (i) Its strong solvatochromism (arising principally from interaction of the cyanide lone pairs with protic solvents) means that the ^{1}MLCT absorption energy, ^{3}MLCT luminescence energy, intensity and lifetime, and the Ru(II)/Ru(III) redox potential, can all be tuned over a wide range by varying the solvent composition.[2] This means that the ability of $[Ru(bipy)(CN)_4]^{2-}$ to act as, for example, an energy donor or an electron donor in its excited state can be controlled by changing the solvent.[3] (ii) Interaction of the cyanide lone pairs with other metal ions in solution likewise allows the properties of the $[Ru(bipy)(CN)_4]^{2-}$ unit to be varied, to a much greater extent than can be achieved by solvation alone.[4] The effect on the photophysical properties of $[Ru(bipy)(CN)_4]^{2-}$ arising from coordination of its cyanide

* To whom correspondence should be addressed. Email: m.d.ward@sheffield.ac.uk.

(1) Ward, M. D. *Coord. Chem. Rev.* **2006**, *250*, 3128.

(2) (a) Bignozzi, C. A.; Chiorboli, C.; Indelli, M. T.; Scandola, M. A. R.; Varani, G.; Scandola, F. *J. Am. Chem. Soc.* **1986**, *108*, 7872. (b) Habib Jiwan, J. L.; Wegewijs, B.; Indelli, M. T.; Scandola, F.; Braslavsky, S. E. *Recl. Trav. Chim. Pays-Bas* **1995**, *114*, 542. (c) Timpson, C. J.; Bignozzi, C. A.; Sullivan, B. P.; Kober, E. M.; Meyer, T. J. *J. Phys. Chem.* **1996**, *100*, 2915. (d) Pinheiro, C.; Lima, J. C.; Parola, A. J. *Sens. Actuators, B* **2006**, *114*, 978.

(3) (a) Indelli, M. T.; Ghirotti, M.; Prodi, A.; Chiorboli, C.; Scandola, F.; McClenaghan, N. D.; Puntoriero, F.; Campagna, S. *Inorg. Chem.* **2003**, *42*, 5489. (b) Simpson, N. R. M.; Ward, M. D.; Morales, A. F.; Barigelletti, F. *J. Chem. Soc., Dalton Trans.* **2002**, 2449. (c) Argazzi, R.; Bignozzi, C. A.; Yang, M.; Hasselmann, G. M.; Meyer, G. J. *Nano Lett.* **2002**, *2*, 625.

10.1021/ic701169c CCC: $37.00 © 2007 American Chemical Society
Published on Web 10/02/2007

lone pairs to, for example, a strong Lewis acid like Zn^{2+}, is much greater than the perturbation that can be obtained by the interaction of the cyanides with the $\delta+$ protons of a solvent such as water. Thus, $[Ru(^tBu_2bipy)(CN)_4]^{2-}$ is very weakly luminescent in MeCN, but the addition of Ba^{2+} or Zn^{2+} salts switches on a strong, long-lived ($\tau \approx 1$ μs) emission in the 540−600 nm region.[4] (iii) The ability of the cyanide lone pairs to coordinate to other metal ions allows $[Ru(bipy)(CN)_4]^{2-}$ to be incorporated in cyanide-bridged coordination networks with additional metal cations;[5,6] we have characterized several $Ln^{3+}/[Ru(bipy)(CN)_4]^{2-}$ networks in which the ^{3}MLCT state of the Ru(II) unit acts as a sensitizer of near-infrared luminescence from lanthanide(III) ions such as Yb(III) and Nd(III).[6] (iv) The ability of the cyanide groups to act as hydrogen-bond acceptors provides a mechanism for $[Ru(bipy)(CN)_4]^{2-}$ to become incorporated into supramolecular arrays, allowing photoinduced energy- or electron-transfer to other components in hydrogen-bonded assemblies.[7] (v) Finally, the cyanide groups provide a useful IR-active reporter group that can be used to monitor excited-state processes using ultrafast time-resolved IR spectroscopy because the position of the ν(CN) band is sensitive to changes in the electron distribution of the complex in its excited state.[8]

The immense value of $[Ru(bipy)(CN)_4]^{2-}$ in the field of supramolecular photochemistry has now prompted us to examine the Os(II) analogue $[Os(bipy)(CN)_4]^{2-}$, a complex that, surprisingly, has so far received only a single report in the literature[9] but which is potentially as useful as $[Ru(bipy)(CN)_4]^{2-}$. The comparison between other Os(II) and Ru(II) complexes with polypyridyl-based ligand sets is instructive. Although $[Ru(bipy)_3]^{2+}$ has the higher-energy and longer-lived excited state, and shows more intense luminescence, $[Os(bipy)_3]^{2+}$ and its analogues have received considerable attention, for example as energy acceptors in Ru−Os dyads displaying Ru → Os energy transfer.[10] Os(II)-polypyridyl complexes are also of particular interest as sensitizers whose absorption (and emission) spectra extend further into the red than do those of Ru(II)-based complexes,[11] which makes them valuable as red emitters in OLEDs.[11a]

Accordingly, in this article we describe the syntheses of $[Os(bipy)(CN)_4]^{2-}$ and some related diimine complexes; crystal structures of several members of the series, including some coordination networks; and the redox, spectroelectrochemical, and photophysical properties of the complexes, including illustrations of how the inherently weak and short-lived luminescence can be massively boosted using the metallochromism effect that we described earlier for $[Ru(bipy)(CN)_4]^{2-}$.[4]

Results and Discussion

Syntheses. The published synthesis of $[Os(bipy)(CN)_4]^{2-}$ involves the reaction of bipy with $[Os(CN)_6]^{4-}$ in aqueous MeOH.[9] Using this method, we isolated several complexes of the type $[Os(NN)(CN)_4]^{2-}$ in good yield, with NN = 1,10-phenanthroline (phen), 2,2′-bipyrimidine (bpym), and 4,4′-$^tBu_2$-2,2′-bipyridine ($^tBu_2$bpy) in addition to the original complex with 2,2′-bipyridine (bipy). Following chromatographic purification on Sephadex-G10, these complexes were all isolated as their Na^+ salts (for NN = bipy, phen, bpym), which are soluble in water and dmso, sparingly soluble in MeOH, and insoluble in other common organic solvents. These could simply be converted to their PPN^+ salts (PPN^+ is $Ph_3P{=}N{=}PPh_3^+$), which are soluble in polar organic solvents, by precipitation of the sodium salts from water using PPN^+Cl^-. The only exception to this is the sodium salt of the relatively hydrophobic complex $[Os(^tBu_2bpy)(CN)_4]^{2-}$, which was not purified but converted directly to the PPN^+ salt. The complexes were satisfactorily characterized on the basis of their ES mass spectra, elemental analyses, and IR spectra, which showed the expected pattern of ν-(CN) stretches, similar to those observed for $[Ru(diimine)(CN)_4]^{2-}$ complexes.[2]

Structural Studies. Several of the complexes have been structurally characterized, as their Na^+ salts or their PPN^+ salts or both. In all of the cases, the structure and geometry of the basic octahedral Os(II) core is unremarkable and will not be dwelt on in detail; the features of interest are the second coordination sphere (hydrogen bonding of solvent molecules and formation of infinite coordination networks in the case of the Na^+ complexes), and the relevant features are summarized briefly below for each complex.

(4) Lazarides, T.; Easun, T. L.; Veyne-Marti, C.; Alsindi, W. Z.; George, M. W.; Deppermann, N.; Hunter, C. A.; Adams, H.; Ward, M. D. *J. Am. Chem. Soc.* **2007**, *129*, 4014.

(5) (a) Adams, H.; Alsindi, W. Z.; Davies, G. M.; Duriska, M. B.; Easun, T. L.; Fenton, H. E.; Herrera, J.-M.; George, M. W.; Ronayne, K. L.; Sun, X.-Z.; Towrie, M.; Ward, M. D. *Dalton Trans.* **2006**, 39. (b) Baca, S. G.; Adams, H.; Ward, M. D. *CrystEngComm.* **2006**, *8*, 635. (c) Herrera, J.-M.; Baca, S.; Adams, H.; Ward, M. D. *Polyhedron* **2006**, *25*, 869.

(6) (a) Davies, G. M.; Pope, S. J. A.; Adams, H.; Faulkner, S.; Ward, M. D. *Inorg. Chem.* **2005**, *44*, 4656. (b) Herrera, J.-M.; Pope, S. J. A.; Adams, H.; Faulkner, S.; Ward, M. D. *Inorg. Chem.* **2006**, *45*, 3895. (c) Herrera, J.-M.; Ward, M. D.; Adams, H.; Pope, S. J. A.; Faulkner, S. *Chem. Commun.* **2006**, 1851.

(7) (a) Simpson, N. R. M.; Ward, M. D.; Morales, A. F.; Ventura, B.; Barigelletti, F. *J. Chem. Soc., Dalton Trans.* **2002**, 2455. (b) Derossi, S.; Adams, H.; Ward, M. D. *Dalton Trans.* **2007**, 33. (c) Loiseau, F.; Marzanni, G.; Quici, S.; Indelli, M. T.; Campagna, S. *Chem. Commun.* **2003**, 286. (d) Bergamini, G.; Saudan, C.; Ceroni, P.; Maestri, M.; Balzani, V.; Gorka, M.; Lee, S.-K.; van Heyst, J.; Vögtle, F. *J. Am. Chem. Soc.* **2004**, *126*, 16466. (e) Pina, F.; Parola, A. J. *Coord. Chem. Rev.* **1999**, *185−186*, 149.

(8) Alsindi, W. Z.; Easun, T. L.; Sun, X.-Z.; Ronayne, K. L.; Towrie, M.; Herrera, J.-M.; George, M. W.; Ward, M. D. *Inorg. Chem.* **2007**, *46*, 3696.

(9) García Posse, M. E.; Katz, N. E.; Baraldo, L. M.; Polonuer, D. D.; Colombano, C. G.; Olabe, J. A. *Inorg. Chem.* **1995**, *34*, 1830.

(10) (a) De Cola, L.; Belser, P.; von Zelewsky, A.; Vögtle, F. *Inorg. Chim. Acta* 2007, **360**, 775. (b) Welter, S.; Salluce, N.; Belser, P.; Groeneveld, M.; De Cola, L. *Coord. Chem. Rev.* **2005**, *249*, 1360. (c) Bichenkova, E. V.; Yu, X.; Bhadra, P.; Heissigerova, H.; Pope, S. J. A.; Coe, B. J.; Faulkner, S.; Douglas, K. T. *Inorg. Chem.* **2005**, *44*, 4112. (d) Weldon, F.; Hammarstrom, L.; Mukhtar, E.; Hage, R.; Gunneweg, E.; Haasnoot, J. G.; Reedijk, J.; Browne, W. R.; Guckian, A. L.; Vos, J. G. *Inorg. Chem.* **2004**, *43*, 4471. (e) Rau, S.; Schafer, B.; Schebesta, S.; Grussing, A.; Poppitz, W.; Walther, D.; Duati, M.; Browne, W. R.; Vos, J. G. *Eur. J. Inorg. Chem.* **2003**, 1503. (e) Sauvage, J.-P.; Collin, J.-P.; Chambron, J.-C.; Guillerez, S.; Coudret, C.; Balzani, V.; Barigelletti, F.; De Cola, L.; Flamigni, L. *Chem. Rev.* **1994**, *94*, 993.

(11) (a) Chou, P.-T.; Chi, Y. *Eur. J. Inorg. Chem.* **2006**, 3319. (b) Juris, A.; Balzani, V.; Campagna, S.; Denti, G.; Serroni, S.; Frei, G.; Güdel, H.-U. *Inorg. Chem.* **1994**, *33*, 1491. (c) Pope, S. J. A.; Coe, B. J.; Faulkner, S.; Laye, R. H. *Dalton Trans.* **2005**, 1482. (d) Evans, R. C.; Douglas, P.; Winscom, C. J. *Coord. Chem. Rev.* **2006**, *250*, 2093. (e) Bergman, S. D.; Gut, D.; Kol, M.; Sabatini, C.; Barbieri, A.; Barigelletti, F. *Inorg. Chem.* **2005**, *44*, 7943.

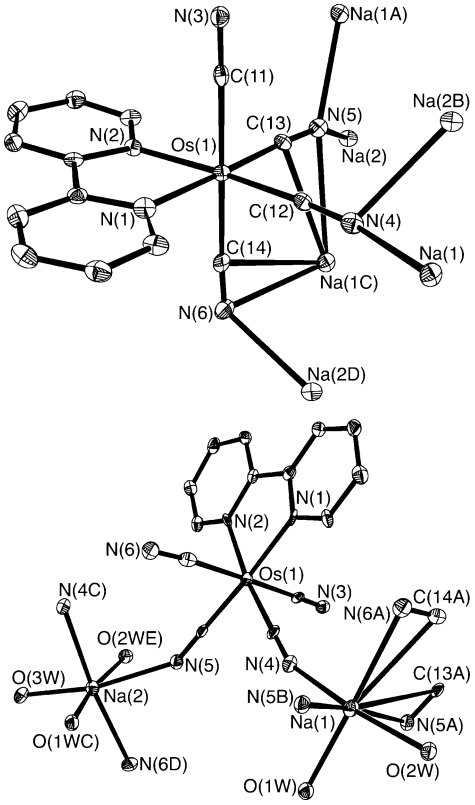

Figure 1. Two views of part of the structure of $Na_2[Os(bipy)(CN)_4]\cdot 4H_2O$: top, emphasising the number of Na^+ cations interacting with each $[Os(bipy)(CN)_4]^{2-}$ anion; bottom, emphasising the environment around each of the independent Na+ ions.

$Na_2[Os(bipy)(CN)_4]\cdot 4H_2O$. Three of the cyanides (containing N(4), N(5), and N(6)) coordinate to Na^+ cations to propagate a coordination network consisting of 2D sheets (Figures 1 and 2). The remaining cyanide, containing N(3), forms hydrogen-bonding interactions with O(1W), O(2W), and O(4W) from different asymmetric units, with nonbonded N···O separations of 3.10, 3.00, and 2.86 Å, respectively. The modes of coordination of the cyanides to Na^+ vary from conventional end-on, with the terminal cyanide lone pair coordinated to one Na^+ ion or bridging two, to a side-on interaction in which the electrons in the CN triple bond interact with the electropositive Na^+ ion. In the case of side-on bonding, the Na···N (and associated Na···C) distances are considerably longer than observed in end-on CN···Na bonding. We have observed this type of side-on coordination of cyanides to alkali-metal cations before, and it becomes more dominant as the alkali-metal ion gets larger and less electropositive.[4,6a] Taking a side-on cyanide ligand as occupying a single coordination site (cf. π-bonding coordination of alkenes/alkynes), Na(1) is six coordinate from two side-on cyanides, two end-on cyanides, and two water ligands. Na(2), in contrast, has six monodentate ligands, three end-on cyanide nitrogen donors, and three water ligands. Part (a) of Figure 1 shows the way in which each $[Os(bipy)(CN)_4]^{2-}$ unit interacts with several Na^+ ions; part (b) of Figure 1 emphasizes the coordination geometry around each independent Na^+ ion. Figure 2 shows a view of the 2D sheet, which lies in the crystallographic *ab* plane, seen edge-on looking along the *a* axis. It will be apparent that the core of the layer is based on a water-bridged network of Na^+ ions, capped above and below by $[Os(bipy)(CN)_4]^{2-}$ units which interact with the Na^+ ions via their cyanide groups.

$Na_2[Os(phen)(CN)_4]\cdot 5H_2O$. This has a quite different supramolecular structure from the bipy complex (above), forming 1D chains containing $Os_2Na_2(\mu-CN)_4$ diamonds (Figures 3, 4). The two equatorial cyanide ligands of each $[Os(phen)(CN)_4]^{2-}$ unit each bind end-on to a different Na(1) ion, and simultaneously both bind side-on to the same Na(2) ion which is sandwiched between them. Figure 4 shows how this results in a 1D chain. Interestingly, Na(1) interacts with cyanide donors solely in an end-on manner and has a regular octahedral coordination geometry arising from four such cyanide nitrogen donors in an approximate plane, and two oxygen donors from (bridging) water ligands. In contrast Na(2) sits at the center of the $Os_2Na_2(\mu-CN)_4$ squares defined by the Os(1) and Na(1) ions, and consequently interacts with the four cyanide ligands describing the edge of each square solely in a side-on manner. Assuming that each edge-on cyanide formally occupies one coordination site, Na(2) is also six-coordinate, from four side-on cyanides and two (bridging) water ligands which connect Na(1) and Na(2). The central 'spine' of this chain consists of a sequence of alternating Na(1) and Na(2) centers connected by water

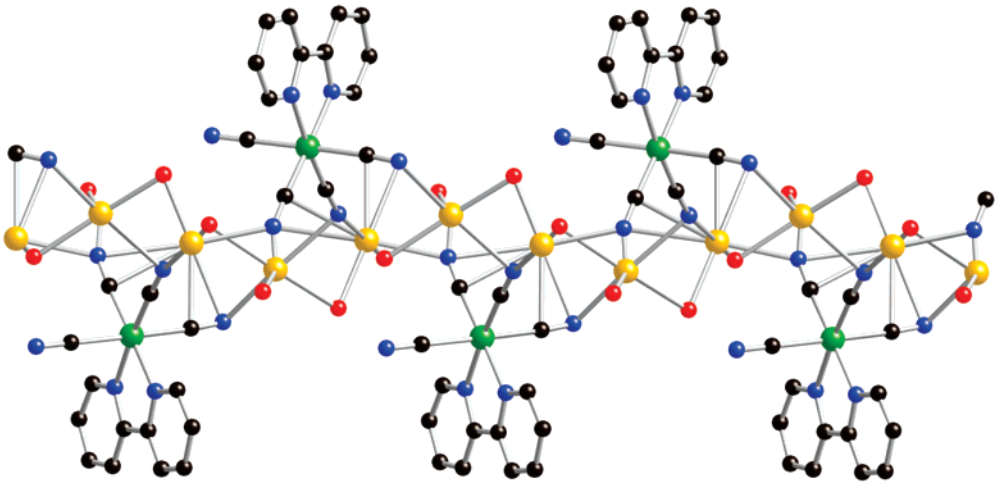

Figure 2. Edge-on view of a 2D sheet in $Na_2[Os(bipy)(CN)_4]\cdot 4H_2O$ (osmium, green; sodium, orange; oxygen, red; nitrogen, blue).

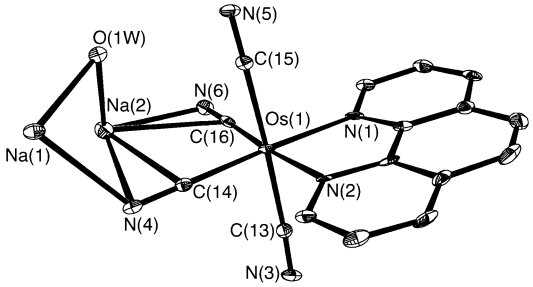

Figure 3. Structure of the asymmetric unit of $Na_2[Os(phen)(CN)_4]\cdot 5H_2O$.

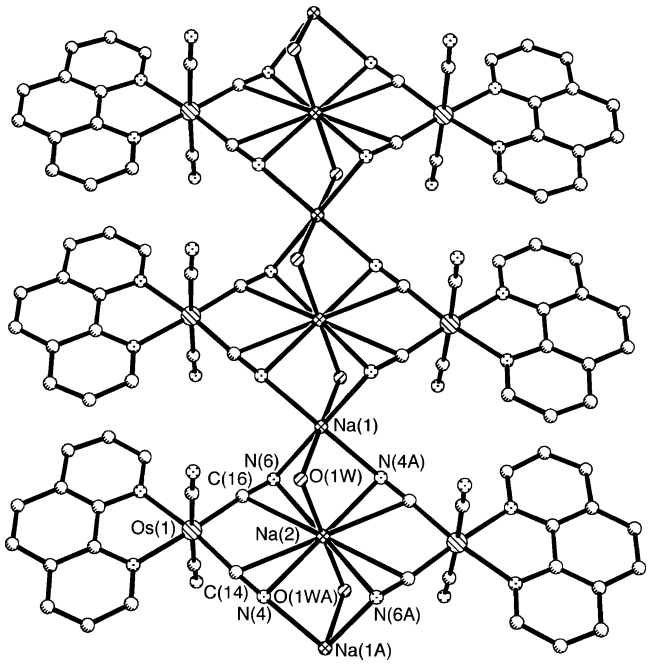

Figure 4. 1D chain structure of $Na_2[Os(phen)(CN)_4]\cdot 5H_2O$; note the two different Na^+ environments, one bound end-on by cyanides [Na(1)] and the other bound side-on [Na(2)].

bridges. This assembly contains equal numbers of $[Os(phen)(CN)_4]^{2-}$ units and Na^+ ions; charge balance is provided by one additional Na^+ ion *per* $[Os(phen)(CN)_4]^{2-}$ unit [Na(3), not shown] which forms $[\{Na(H_2O)_3\}_2(\mu-H_2O)_2]^{2+}$ dimers.

$Na_2[Os(bpym)(CN)_4]\cdot nH_2O$ ($n = 4, 8$). Crystallization of $Na_2[Os(bpym)(CN)_4]$ from aqueous solution afforded three different types of crystal, which proved to differ in the number of water molecules associated with each formula unit. This apparently trivial difference resulted in big changes in the supramolecular structure, and the structures of the tetra- and octa-hydrates are described here.

$Na_2[Os(bpym)(CN)_4]\cdot 4H_2O$ forms a 3D infinite network in which Na^+ ions are coordinated not only by cyanide ligands (in both end-on and side-on coordination modes), but also by the second site of the bipyrimidine ligand of the $[Os(bpym)(CN)_4]^{2-}$ unit. The asymmetric unit, with a few additional atoms to complete the coordination sphere around each metal ion, is shown in Figure 5. Each $[Os(bpym)(CN)_4]^{2-}$ unit uses three of its four cyanide ligands to interact with Na^+ ions. The cyanides containing N(6) and N(7) both act as side-on donors to Na(2) which lies in the pocket between the two cyanides, and N(7) provides an additional end-on coordination to Na(1), which is also coordinated by the

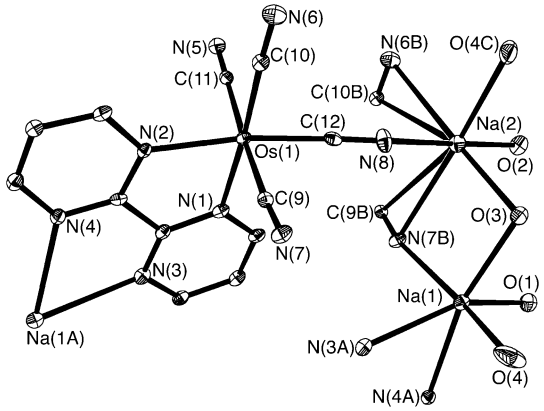

Figure 5. Structure of the asymmetric unit of $Na_2[Os(bpym)(CN)_4]\cdot 4H_2O$.

vacant bipyrimidine coordination site of $[Os(bpym)(CN)_4]^{2-}$. The third coordinating cyanide group, containing N(8), provides end-on coordination to Na(2). Thus Na(1) and Na(2) are both formally six-coordinate, taking a side-on cyanide as occupying one coordination site. Na(1) is coordinated by a bipyrimidine chelate, one end-on cyanide [N(7)], and three water molecules as ligands, one of which [O(3)] bridges to the adjacent Na(2) center. Na(2) is coordinated by two side-on cyanides [involving N(6) and N(7)], an end-on cyanide [N(8)] and two water ligands. Figure 6 shows a view of the resulting 3D network structure, viewed down the crystallographic *a* axis.

In $Na_2[Os(bpym)(CN)_4]\cdot 8H_2O$, in contrast, the additional water molecules are used to saturate the coordination sphere of the Na^+ ions, such that the secondary diimine site of each $[Os(bpym)(CN)_4]^{2-}$ unit is not involved in direct coordination to a Na^+ ion (Figure 7). Instead, the crystallographically independent Na^+ ions are associated into an infinite 1D chain, with Na(1) and Na(2) centers alternating, with three water molecules bridging each pair of adjacent metals. Thus, each Na^+ center is six-coordinate and roughly octahedral. The $[Os(bpym)(CN)_4]^{2-}$ unit interacts with this chain via the hydrogen bonding of water molecules [O(2)] to both of the (symmetry equivalent) non-coordinated bipyrimidine nitrogen atoms, with the N(2)···O(2) separation being 2.91 Å; this hydrogen bond is nearly linear, with the O−H···N angle being 169°. In addition, the lattice water molecule [O(4)] is involved in hydrogen-bonding interactions with O(1) and O(3) of the Na^+/water chain (O···O separations of 2.85 and 2.84 Å, respectively) and a cyanide atom N(3) from an adjacent asymmetric unit [O(4)···N(3), 2.92 Å].

$(PPN)_2[Os(^tBu_2bipy)(CN)_4]\cdot 2H_2O\cdot(Me_2CO)$. In this case, with a non-coordinating organic cation, the main supramolecular structure is provided by hydrogen bonding between some of the cyanide ligands of the $[Os(^tBu_2bipy)(CN)_4]^{2-}$ anion and lattice water molecules. Figure 8 includes the relevant interactions, with nonbonded N···O separations as follows: N(4)···O(1), 2.77; N(6)···O(2), 3.00; and N(5)···O(2), 3.05 Å. The cyanide nitrogen atoms are also involved in CN···HC hydrogen bonds with the phenyl rings of the $(PPN)^+$ cations, of which the shortest is C(132)···N(6) at 3.15 Å.

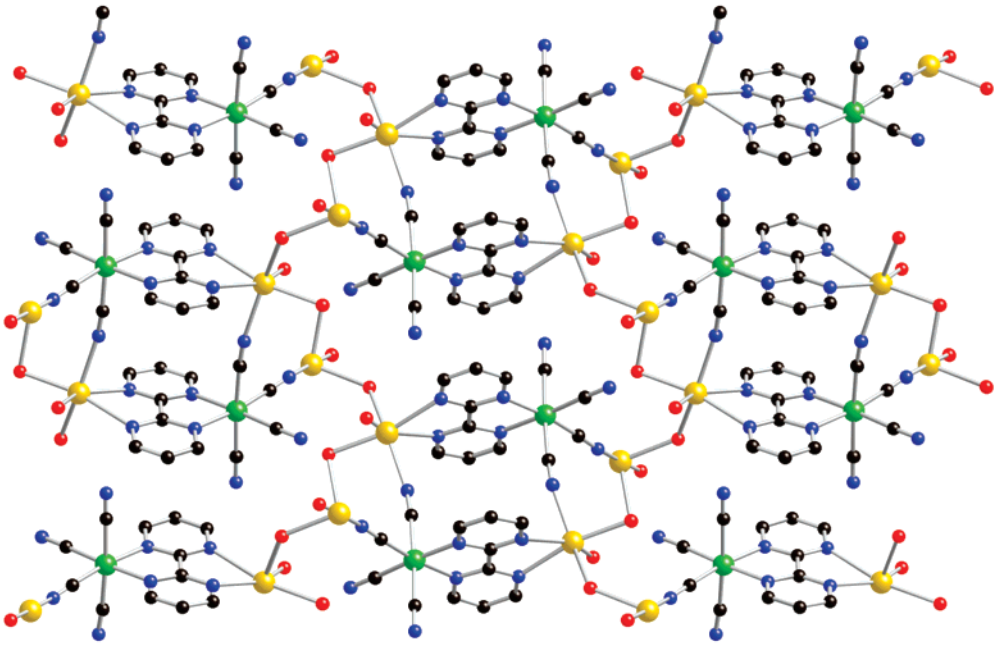

Figure 6. Part of the 3D network structure of $Na_2[Os(bpym)(CN)_4]\cdot 4H_2O$ (osmium, green; sodium, orange; oxygen, red; nitrogen, blue).

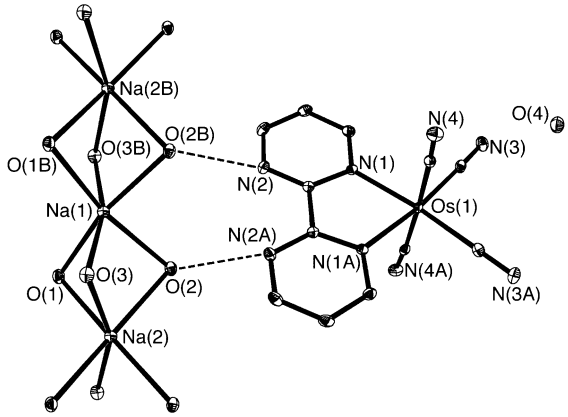

Figure 7. View of the crystal structure of $Na_2[Os(bpym)(CN)_4]\cdot 8H_2O$, emphasising the hydrogen-bonding interaction between the cyanoosmate anion and the Na^+/water cationic chain.

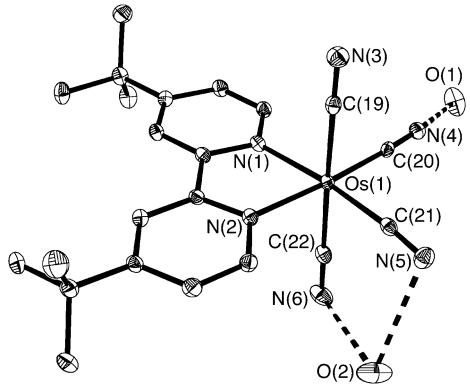

Figure 8. View of the complex anion in the crystal structure of $(PPN)_2[Os(^tBu_2bipy)(CN)_4]\cdot 2H_2O\cdot(Me_2CO)$.

Electronic Absorption and Luminescence Spectra; Solvatochromism. In organic solvents, the UV−vis absorption spectra of $[Os(bipy)(CN)_4]^{2-}$ and $[Os(^tBu_2bipy)(CN)_4]^{2-}$ show three features in or close to the visible region: a strong absorption at ca. 390 nm; a second absorption at ca. 550 nm, which (in three of the four cases examined) is slightly less intense; and a much weaker area of absorbance at ca. 710 nm (Table 3 for a summary of UV−vis absorption spectra). The two higher-energy features are very similar to what is observed in analogous Ru(II) complexes[1,2,4] and can therefore both be assigned as spin-allowed ^{1}MLCT absorptions to different π^* levels of the diimine ligand. The much-weaker feature at lower energy, which has no counterpart in the absorption spectra of $[Ru(bipy)(CN)_4]^{2-}$ complexes, can be assigned as a spin-forbidden ^{3}MLCT absorption. There is an obvious parallel with the absorption spectra of other Os(II) versus Ru(II) bipyridine complexes, in which a low-energy spin-forbidden ^{3}MLCT absorption is apparent for the Os(II) complexes but not for the Ru(II) complexes.[12] $[Os(bpym)(CN)_4]^{2-}$ shows similar behavior, although the three absorption features are all red-shifted because of the lower-energy π^* orbitals of the bpym ligand compared to bipy/ ^{t}Bu$_2$bipy; $[Os(phen)(CN)_4]^{2-}$ likewise shows similar behavior although the higher-energy ^{1}MLCT transition is less intense than the lower-energy one.

In water, all three MLCT absorptions shift to higher energy. The extent of the shift is such that the highest-energy transition for $[Os(bipy)(CN)_4]^{2-}$ and $[Os(phen)(CN)_4]^{2-}$ becomes obscured by $\pi-\pi^*$ transitions in the UV region; the lower of the two ^{1}MLCT absorptions have moved up to 415 and 405 nm respectively, and the ^{3}MLCT absorption is apparent as a shoulder at ca. 520 nm in each case. For $[Os(bpym)(CN)_4]^{2-}$, the absorption maxima were lower in energy to start with but are blue-shifted to a comparable extent, with the highest-energy ^{1}MLCT absorption moving from 430 nm in MeCN to 360 nm in water and the lower

(12) (a) Kober, E. M.; Caspar, J. V.; Sullivan, B. P.; Meyer, T. J. *Inorg. Chem.* **1988**, *27*, 4587. (b) Della Ciana, L.; Dressick, W. J.; Sandrini, D.; Maestri, M.; Ciano, M. *Inorg. Chem.* **1990**, *29*, 2792. (c) Decurtins, S.; Felix, F.; Ferguson, J.; Güdel, H.; Ludi, A. *J. Am. Chem. Soc.* **1980**, *102*, 4102.

Table 1. Selected Bond Distances (Angstroms) for the Five Crystal Structures

(a) $Na_2[Os(bipy)(CN)_4]\cdot 4H_2O$			
Os(1)−C(12)	1.974(6)	Na(1)−N(5)#2	2.970(6)
Os(1)−C(13)	1.980(6)	Na(1)−C(13)#2	3.098(6)
Os(1)−C(11)	2.038(6)	Na(1)−Na(2)#1	3.256(3)
Os(1)−C(14)	2.055(6)	Na(1)−Na(2)#2	3.295(3)
Os(1)−N(2)	2.104(5)	Na(2)−O(1W)#3	2.380(5)
Os(1)−N(1)	2.111(5)	Na(2)−O(3W)	2.427(5)
Na(1)−O(2W)	2.319(5)	Na(2)−O(2W)#4	2.473(5)
Na(1)−O(1W)	2.386(5)	Na(2)−N(5)	2.505(6)
Na(1)−N(4)	2.411(6)	Na(2)−N(6)#5	2.507(6)
Na(1)−N(5)#1	2.568(6)	Na(2)−N(4)#3	2.637(5)
Na(1)−N(6)#2	2.716(6)	Na(2)···Na(1)#4	3.256(3)
Na(1)−C(14)#2	2.942(6)	Na(2)···Na(1)#3	3.295(3)
(b) $Na_2[Os(phen)(CN)_4]\cdot 5H_2O$			
Os(1)−C(14)	1.980(10)	Na(2)−N(6)	2.554(9)
Os(1)−C(16)	1.986(12)	Na(2)−C(16)	2.798(11)
Os(1)−C(15)	2.044(10)	Na(2)−N(4)	2.919(10)
Os(1)−C(13)	2.046(11)	Na(2)−C(14)	3.041(11)
Os(1)−N(1)	2.104(9)	Na(3)−O(5W)	2.288(9)
Os(1)−N(2)	2.138(9)	Na(3)−O(2W)	2.340(8)
Na(1)−N(6)#1	2.383(9)	Na(3)−O(3W)#5	2.344(9)
Na(1)−O(1W)	2.465(8)	Na(3)−O(4W)	2.425(9)
Na(1)−N(4)	2.606(9)	Na(3)−O(3W)	2.509(9)
Na(2)−O(1W)	2.303(8)		
(c) $Na_2[Os(bpym)(CN)_4]\cdot 4H_2O$			
Os(1)−C(10)	1.976(5)	Na(1)−N(4)#1	2.529(5)
Os(1)−C(12)	1.985(5)	Na(1)−N(3)#1	2.593(5)
Os(1)−C(11)	2.055(5)	Na(2)−O(3)	2.372(4)
Os(1)−C(9)	2.062(5)	Na(2)−O(2)	2.375(4)
Os(1)−N(1)	2.107(4)	Na(2)−O(4)#4	2.431(5)
Os(1)−N(2)	2.110(4)	Na(2)−N(7)#3	2.823(5)
Na(1)−O(1)	2.410(4)	Na(2)−N(6)#3	2.957(5)
Na(1)−O(3)	2.415(4)	Na(2)−C(9)#3	3.045(6)
Na(1)−O(4)	2.428(5)	Na(2)−C(10)#3	3.121(6)
Na(1)−N(7)#3	2.482(5)		
(d) $Na_2[Os(bpym)(CN)_4]\cdot 8H_2O$			
Os(1)−C(5)	1.9948(16)	Na(1)−O(3)	2.4112(13)
Os(1)−C(6)	2.0468(17)	Na(2)−O(1)	2.4005(13)
Os(1)−N(1)	2.1088(13)	Na(2)−O(2)	2.4195(13)
Na(1)−O(2)	2.3774(13)	Na(2)−O(3)	2.4328(13)
Na(1)−O(1)	2.3807(13)		
(e) $(PPN)_2[Os(^tBu_2bipy)(CN)_4]\cdot 2H_2O\cdot(Me_2CO)$			
Os(1)−C(21)	1.993(3)	Os(1)−C(19)	2.061(3)
Os(1)−C(20)	1.997(3)	Os(1)−N(2)	2.102(2)
Os(1)−C(22)	2.036(3)	Os(1)−N(1)	2.103(2)

(a) Symmetry transformations used to generate equivalent atoms: #1 $-x-1, y-1/2, -z+3/2$. #2 $x+1, y, z$. #3 $x-1, y, z$. #4 $-x-1, y+1/2, -z+3/2$. #5 $-x-2, y+1/2, -z+3/2$. #6 $-x-2, y-1/2, -z+3/2$. (b) Symmetry transformations used to generate equivalent atoms: #1 $x+1, y, z$. #2 $-x+1, -y, -z$. #3 $-x+2, -y, -z$. #4 $x-1, y, z$. #5 $-x+2, -y+1, -z+2$. (c) Symmetry transformations used to generate equivalent atoms: #1 $-x+1, -y+1, -z$. #2 $x-1, y, z$. #3 $x+1, y, z$. #4 $-x+3/2, y+1/2, -z+1/2$. #5 $-x+3/2, y-1/2, -z+1/2$.

two behaving similarly (Figure 9). This solvatochromism, arising from hydrogen-bonding interactions between water molecules and cyanide ligands, is exactly comparable to that observed for the analogous Ru(II) complexes.[1,2]

The luminescence (Table 4) of $[Os(bipy)(CN)_4]^{2-}$ is much weaker than that observed for $[Ru(bipy)(CN)_4]^{2-}$, being reported previously as undetectable in organic solvents at room temperature and very weak in water [at 1.81 eV (= 685 nm) with $\tau \approx 3$ ns].[9] We could not detect any significant emission from MeCN solutions using a conventional luminescence spectrometer with a long wavelength limit of 900 nm, but we could, however, see weak luminescence at ca. 980 nm from all of the complexes except $[Os(bpym)(CN)_4]^{2-}$ in MeCN using laser excitation and a near-IR CCD camera (Figure 10). The quantum yields are too low to determine accurately but are much less than that of $[Os(bipy)(CN)_4]^{2-}$ in water, for which ϕ was estimated as $<5 \times 10^{-4}$. In contrast, the emission from $[Ru(bipy)(CN)_4]^{2-}$ is at ~800 nm in MeCN,[2c] so we are seeing here the usual lower energy for the ^{3}MLCT emission from Os(II) complexes compared to their Ru(II) counterparts because of the higher energy of the Os(II)-based d orbitals.[12]

In water, $[Os(phen)(CN)_4]^{2-}$ shows comparable behavior to $[Os(bipy)(CN)_4]^{2-}$, with a weak red emission at 685 nm ($\tau = 12$ ns) for the phen complex compared to $\lambda_{em} = 695$ nm and $\tau = 4$ ns for the bipy complex (Figure 10). The longer lifetime and higher quantum yield for emission from the phen complex is due to the greater rigidity of the phen ligand compared to bipy, which inhibits some nonradiative deactivation pathways. $[Os(bpym)(CN)_4]^{2-}$ (like the Ru(II) analogue)[5a] is completely nonluminescent in water at room temperature, and $(PPN)_2[Os(^tBu_2bipy)(CN)_4]$ is not water soluble.

Luminescence also occurs at 77 K in EtOH/MeOH glasses (except, again, for $[Os(bpym)(CN)_4]^{2-}$). Consistent with the earlier report,[9] we observed a broad, weak emission from $[Os(bipy)(CN)_4]^{2-}$ with a maximum at 670 nm under these conditions; for $[Os(^tBu_2bipy)(CN)_4]^{2-}$ and $[Os(phen)(CN)_4]^{2-}$ under the same conditions, we observed emission maxima at 640 and 655 nm, respectively. From these maxima at 77 K, we can estimate the ^{3}MLCT energies of the bipy, phen, and ^{t}Bu$_2$bipy complexes as 14900, 15300, and 15600 cm^{-1} respectively under these conditions.

Metallochromism of $[Os(^tBu_2bipy)(CN)_4]^{2-}$ in MeCN. The very weak luminescence of $[Os(bipy)(CN)_4]^{2-}$-type complexes in fluid solution apparently limits their utility as luminophores or energy donors. However, we observed recently that the luminescence of $[Ru(^tBu_2bipy)(CN)_4]^{2-}$, which is almost nonexistent in non-hydrogen bonding solvents such as MeCN, is substantially boosted in energy, intensity, and lifetime by the addition of salts of Lewis-acidic metal ions to the solution.[4] In a noncompetitive solvent, the coordination of these cations to the cyanide nitrogen atoms of $[Ru(^tBu_2bipy)(CN)_4]^{2-}$ has an effect comparable in origin to the solvatochromism induced by hydrogen bonding to the $\delta+$ protons of water, but much greater in magnitude, resulting in the luminescence from $[Ru(^tBu_2bipy)(CN)_4]^{2-}$ being blue-shifted up to a wavelength of ca. 540 nm and lifetimes in the microsecond region being observed.[4] We show here how the luminescence of $[Os(^tBu_2bipy)(CN)_4]^{2-}$ can similarly be substantially enhanced in the same way by exploiting this metallochromism, using the ions Na^+, Ba^{2+}, and Zn^{2+}.

The effects on the UV−vis absorption spectrum of titrating NaI into a solution of $(PPN)_2[Os(^tBu_2bipy)(CN)_4]$ in MeCN are shown in part (a) of Figure 11. All three MLCT absorption bands steadily blue-shift as the concentration of Na^+ ions increases. The weak lowest-energy ^{3}MLCT absorption moves from 715 nm to become a shoulder at ca. 550 nm; the lower-energy ^{1}MLCT absorption band starts at 548 nm and shifts to 440 nm; and the highest-energy ^{1}MLCT absorption band moves from 376 nm up to 330 nm. This amounts to a blue shift of ca. 4000 cm^{-1} for each transition, resulting in a final absorption spectrum that is similar to that observed for $[Os(bipy)(CN)_4]^{2-}$ in water,[9] albeit slightly less blue-shifted. The origin of this effect is the same as that for the solvatochromism. Coordination of Na^+ ions to the cyanide termini makes the cyanide ligands stronger π

Table 2. Crystal Parameters, Data Collection, and Refinement Details for the Structures in This Article

complex	Na_2[Os(bipy)-$(CN)_4$]·$4H_2O$	Na_2[Os(phen)-$(CN)_4$]·$5H_2O$	Na_2[Os(bpym)-$(CN)_4$]·$4H_2O$	Na_2[Os(bpym)-$(CN)_4$]·$8H_2O$	$(PPN)_2$[Os(^{t}Bu_2bipy)-$(CN)_4$]·$2H_2O$·(Me_2CO)
formula	$C_{14}H_{16}N_6Na_2O_4Os$	$C_{16}H_{18}N_6Na_2O_5Os$	$C_{12}H_{14}N_8Na_2O_4Os$	$C_{12}H_{22}N_8Na_2O_8Os$	$C_{97}H_{94}N_8O_3OsP_4$
fw	568.51	610.54	570.49	642.56	1733.88
T, K	100(2)	100(2)	100(2)	100(2)	150(2)
cryst syst	orthorhombic	triclinic	monoclinic	monoclinic	triclinic
space group	*P*2(1)2(1)2(1)	$P\bar{1}$	*P*2(1)/n	*C*2/c	$P\bar{1}$
a, Å	6.5897(3)	6.5785(6)	6.6192(5)	6.4420(13)	11.0248(12)
b, Å	10.7397(5)	10.6416(9)	11.4117(11)	29.172(6)	14.6697(15)
c, Å	26.9228(12)	15.6335(13)	23.612(2)	12.046(2)	27.379(3)
α, deg	90	105.243(5)	90	90	96.599(6)
β, deg	90	95.882(5)	92.371(5)	92.84(3)	95.141(6)
γ, deg	90	99.237(5)	90	90	96.108(6)
V, Å^3	1905.36(15)	1030.14(5)	1782.1(3)	2261.0(8)	4350.4(8)
Z	4	2	4	4	2
ρ, g cm^{-3}	1.982	1.968	2.126	1.888	1.324
cryst size, mm^3	0.19 × 0.06 × 0.04	0.22 × 0.11 × 0.04	0.14 × 0.09 × 0.04	0.54 × 0.10 × 0.03	0.43 × 0.14 × 0.04
μ, mm^{-1}	6.770	6.272	7.242	5.732	1.594
data, restraints, params	4347, 0, 238	4161, 0, 274	4145, 0, 244	2600, 0, 142	20204, 14, 1021
Final *R*1, *wR*2	0.0302, 0.0617	0.0554, 0.1333	0.0330, 0.0706	0.0101, 0.0262	0.0317, 0.0911

Table 3. UV−Vis Absorption Data for the Complex Salts in Water and MeCN

complex	solvent	λ_{max}/nm (10^{-3} ϵ/M^{-1} cm^{-1})
[Os(bipy)(CN)$_4$]$^{2-}$	H_2O[a]	520 (sh, ≈0.7);[c] 415 (3.3);[d] 286 (23);[e] 243 (12)[e]
	MeCN[b]	745 (0.7);[c] 558 (2.9);[d] 384 (4.2);[d] 295 (16)[e]
[Os(phen)(CN)$_4$]$^{2-}$	H_2O[a]	520 (sh, ≈0.7);[c] 402 (4.5);[d] 262 (31)[e]
	MeCN[b]	700 (sh, ≈0.9);[c] 543 (4.3);[d] 340 (1.9);[d] 266 (22)[e]
[Os(bpym)(CN)$_4$]$^{2-}$	H_2O[a]	570 (sh, ≈0.7);[c] 420 (sh, ≈4);[d] 359 (6.2);[d] 245 (20)[e]
	MeCN[b]	820 (0.4);[c] 540 (sh, ≈2);[d] 425 (4.3)[d]
[Os(^{t}Bu_2bipy)(CN)$_4$]$^{2-}$	MeCN[b]	705 (0.7);[c] 544 (2.8);[d] 377 (4.3);[d] 295 (17)[e]

[a] The Na^+ salt of the complex was used. [b] The PPN^+ salt of the complex was used. [c] ^{3}MLCT absorption. [d] ^{1}MLCT absorption. [e] $\pi-\pi^*$ absorption.

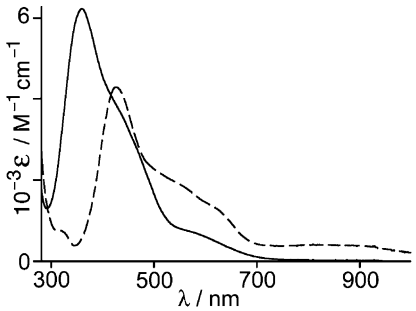

Figure 9. Electronic spectra of Na_2[Os(bpym)(CN)$_4$] in water (solid line) and $(PPN)_2$[Os(bpym)(CN)$_4$] in MeCN (dashed line).

Table 4. Luminescence Data for the Complexes

complex	solvent (temp)	λ_{em}/nm
[Os(bipy)(CN)$_4$]$^{2-}$	H_2O (room temperature)[a]	695 (τ = 4 ns)
	MeCN (room temperature)[b]	980
	EtOH/MeOH (77 K)[b]	670, 720 (sh)
[Os(phen)(CN)$_4$]$^{2-}$	H_2O (room temperature)[a]	685 (τ = 12 ns)
	MeCN (room temperature)[b]	970
	EtOH/MeOH (77 K)[b]	655, 705 (sh)
[Os(^{t}Bu_2bipy)(CN)$_4$]$^{2-}$	MeCN (room temperature)[b]	970
	EtOH/MeOH (77 K)[b]	640

[a] The Na^+ salt of the complex was used. [b] The PPN^+ salt of the complex was used.

acceptors with respect to the Os(II) center, resulting in an increased degree of Os[d(π)] → CN(π^*) back-bonding. This stabilizes the osmium-based d(π) orbitals and results in an increased Os[d(π)] → bipy(π^*) MLCT energy gap. A graph

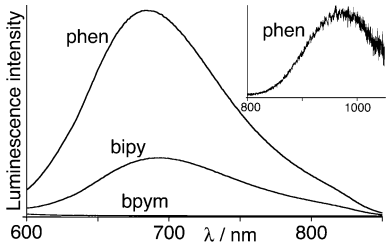

Figure 10. Luminescence spectra of Na_2[Os(diimine)(CN)$_4$] in water (diimine = bipy, phen, bpym), and (inset) of $(PPN)_2$[Os(phen)(CN)$_4$] in MeCN.

of absorbance at 550 nm (the region of maximum change) as a function of added Na^+ gives a curve (inset in Figure 11) that fits well to a 1:2 [Os(^{t}Bu_2bipy)(CN)$_4$]$^{2-}$/Na^+ binding isotherm, with association constants of 1.5(±0.5) and 4.4(±0.4) × 10^4 M^{-1} for binding the first and second Na^+ ions respectively. The data clearly indicate that, surprisingly, the second binding constant is higher than the first one, the opposite of what would be expected on electrostatic grounds. However, the fit to the observed data is excellent, and the calculation reaches the same solution from a variety of different initial values. A possible explanation is the involvement of iodide, such that Na^+ is not binding to [Os(^{t}Bu_2bipy)(CN)$_4$]$^{2-}$/Na^+ on its own but as an NaI ion pair, with the presence of the iodide facilitating the binding of the second Na^+ ion in a cooperative effect.

In parallel with the blue shift of the MLCT absorption maxima, the ^{3}MLCT luminescence from [Os(^{t}Bu_2bipy)(CN)$_4$]$^{2-}$ grows in intensity during the titration (part (b) of Figure 11), starting from essentially nonexistent in the absence of Na^+ ions and ending with a significant emission intensity centered at 730 nm (cf. 685 nm for [Os(bipy)(CN)$_4$]$^{2-}$ in water). Time-resolved measurements at the end of the titration (i.e., when there was no further growth of luminescence intensity) revealed complex multiexponential decay that needed at least three components for a reasonable fit (4, 21, and 60 ns, with relative weightings of 21, 57, and 22%, respectively). This is because [Os(^{t}Bu_2bipy)(CN)$_4$]$^{2-}$ can bind zero, one, two, three, or four Na^+ ions via the cyanide ligands, giving potentially five different species in solution.[4] In addition, for the aggregates with one, two, or three Na^+ ions, more

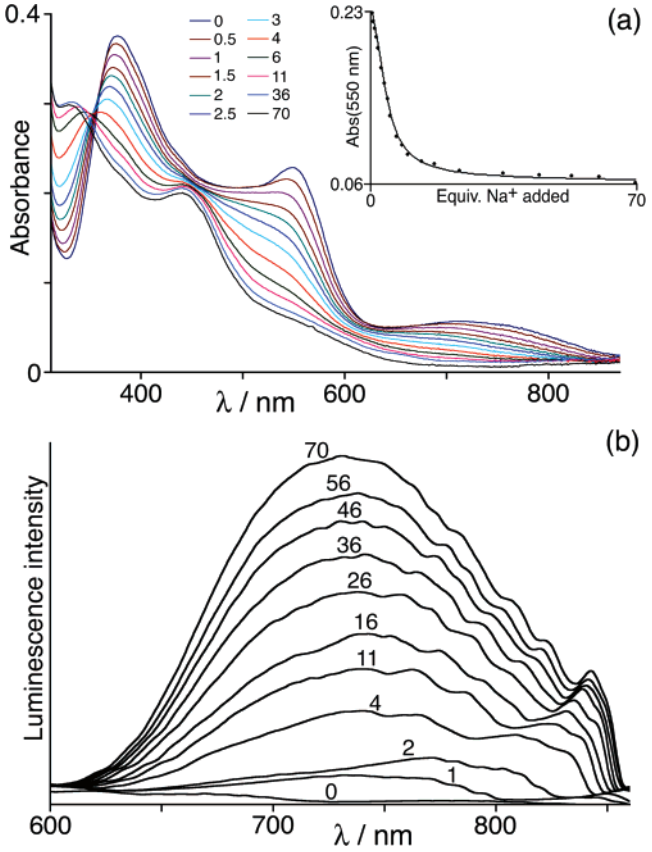

Figure 11. Changes in (a) the UV−vis absorption spectrum and (b) luminescence spectrum of $(PPN)_2$ $[Os(^tBu_2bipy)(CN)_4]$ in MeCN, on titration with NaI. The number of equivs of added NaI are shown for each spectrum. The inset to part (a) shows the curve of luminescence intensity versus the amount of added NaI; the black dots are the measured data, and the solid line is the best fit to these on the basis of the calculated stepwise association constants given in the main text.

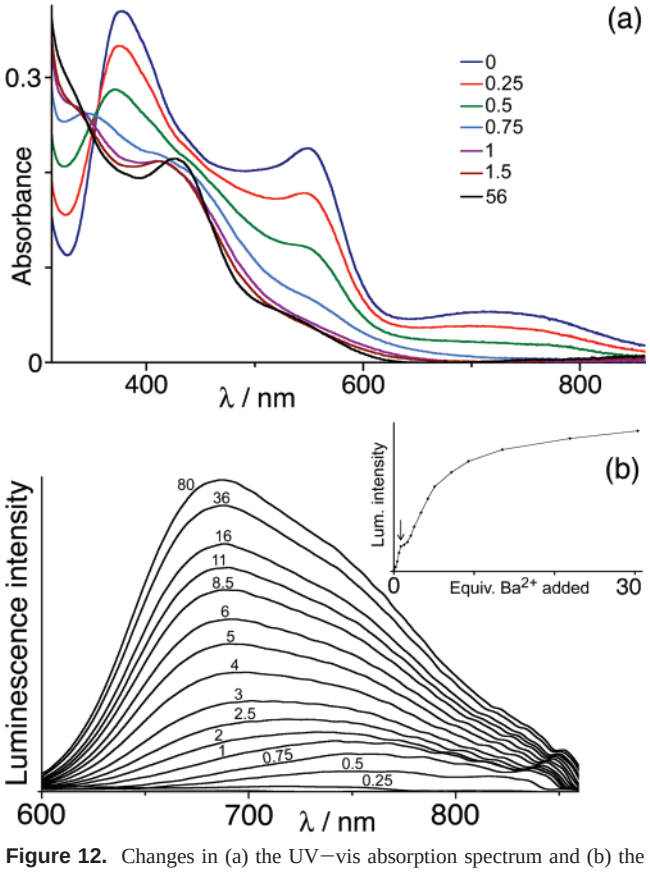

Figure 12. Changes in (a) the UV−vis absorption spectrum and (b) the luminescence spectrum of $(PPN)_2$ $[Os(^tBu_2bipy)(CN)_4]$ in MeCN, on titration with $Ba(ClO_4)_2$. The number of equivs of added $Ba(ClO_4)_2$ are shown for each spectrum.

than one isomer may be present in each case (two, three, and two, respectively) according to whether axial or equatorial cyanide ligands are involved, resulting in a total of nine possible $[Os(^tBu_2bipy)(CN)_4]^{2-}/Na^+$ aggregates. (This ignores the additional possibility that more than one $[Os(^tBu_2bipy)(CN)_4]^{2-}$ ion can interact with the same Na^+ ion, which is unlikely to be a significant issue at high Na^+ concentrations). Thus, the appearance of complex multiexponential luminescence decay is to be expected, and it would be inappropriate to attach too much significance to the values obtained for each individual lifetime component; it is clear, however, that the presence of Na^+ ions coordinated to the cyanide termini of $[Os(^tBu_2bipy)(CN)_4]^{2-}$ in MeCN solution results in the appearance of red ^{3}MLCT luminescence with a lifetime of tens of nanoseconds.

Use of the more strongly Lewis-acidic Ba^{2+} ion had a similar but more dramatic effect. The changes in UV−vis spectra arising from titration of $Ba(ClO_4)_2$ into a solution of $(PPN)_2[Os(^tBu_2bipy)(CN)_4]$ in MeCN are shown in part (a) of Figure 12. All three MLCT absorption bands quickly blue-shift, to a greater extent than we observed using NaI. The weak lowest-energy ^{3}MLCT absorption band moves from 715 nm to become a shoulder at ca. 530 nm; the lower-energy ^{1}MLCT absorption band at 548 nm shifts to 425 nm; and the highest-energy ^{1}MLCT absorption band moves from 376 nm up into the UV region, where it is obscured by the intense $\pi-\pi^*$ transitions associated with the aromatic ligands and the $(PPN)^+$ cation. The average blue shift of these peaks by the end of the titration is ca. 5000 cm^{-1}, and the final absorption spectrum (in the presence of a large excess of Ba^{2+} ions) is comparable to that of $[Os(bipy)(CN)_4]^{2-}$ in water.[9] It is notable that nearly all of the change in the absorption spectrum occurs early, during the addition of the first equiv of Ba^{2+}, with the subsequent changes being much smaller; this contrasts with the much more-gradual change observed with NaI. This indicates that the first association of $[Os(^tBu_2bipy)(CN)_4]^{2-}$ with Ba^{2+} is strong, whereas subsequent binding events are much weaker; this is explicable on simple electrostatic grounds and will be returned to in more detail below.

The effect of the presence of Ba^{2+} ions on the luminescence of $[Os(^tBu_2bipy)(CN)_4]^{2-}$ in MeCN is equally strong and is shown in part (b) of Figure 12. Starting with essentially no luminescence in the visible region, the addition of Ba^{2+} ions results in the appearance of a broad emission band at around 760 nm in the early stages of the titration, which blue-shifts and grows in intensity until, at the end of the titration, there is an intense emission band centered at 685 nm. Time-resolved measurements again show complex multiexponential behavior, for the reasons described above. However at the end of the titration, when there are no further changes to the emission spectrum, the dominant luminescence component has a lifetime of 85 ns.

The graph of how luminescence intensity grows during the titration (inset in part b of Figure 12) is interesting

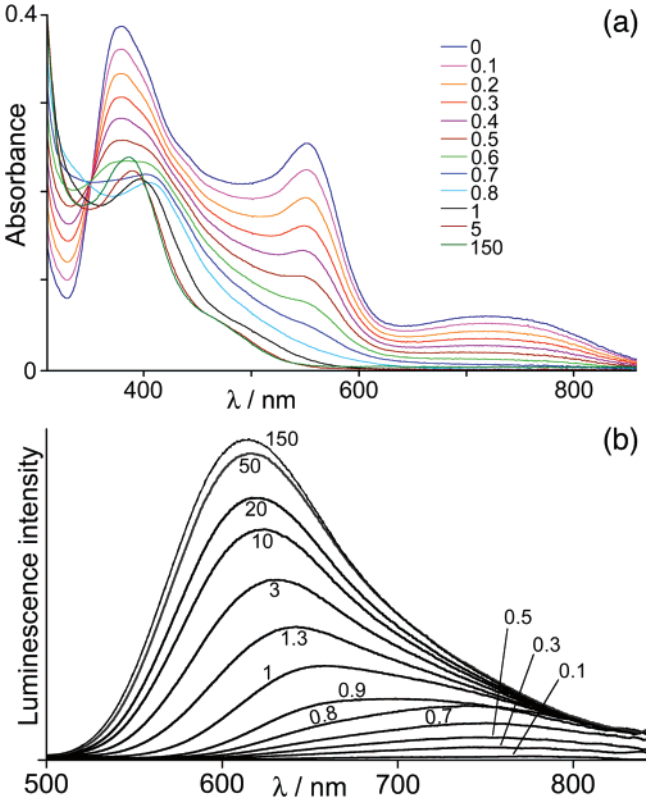

Figure 13. Changes in (a) the UV−vis absorption spectrum and (b) the luminescence spectrum of (PPN)$_2$ [Os(^{t}Bu$_2$bipy)(CN)$_4$] in MeCN, on titration with Zn(ClO$_4$)$_2$·6H$_2$O. The number of equivs of added Zn(ClO$_4$)$_2$·6H$_2$O are shown for each spectrum.

because it clearly reveals the presence of multiple, distinct binding events. The general shape of the curve, an essentially linear increase in emission intensity during the addition of the first equiv of Ba^{2+}, with a sudden discontinuity (marked by the arrow in the figure) and a sigmoidal growth of luminescence intensity thereafter, is similar to what we observed in the titration of [Ru(^{t}Bu$_2$bipy)(CN)$_4$]$^{2-}$ with various metal cations.[4] It can be interpreted in the same way, as a strong first binding event, which is essentially complete after the addition of the first equiv of Ba^{2+}, followed by three weaker binding events: a 1:4 host/guest ratio is the only way to fit the shape of this curve. In this case, the fit was relatively insensitive to substantial variations in the stepwise binding constants, so we cannot provide reliable quantitative data, but we just note that the shape of the curve implies the binding of a maximum of four Ba^{2+} cations, one to each cyanide site.[4]

The effect of adding Zn^{2+} ions is comparable, but the shifts are larger as Zn^{2+} is a stronger Lewis acid than Ba^{2+} because of its smaller ionic radius. The shifts in the UV−vis spectrum are shown in part (a) of Figure 13. The spectral changes are linear with amount of added Zn^{2+} until 1 equiv has been added, with almost no changes thereafter, implying that the initial 1:1 adduct forms first with a high stability constant (much greater than the reciprocal of the concentration, i.e., $\gg 2 \times 10^4$ M^{-1}). The weak lowest-energy ^{3}MLCT absorption band moves from 715 nm to become a shoulder at ca. 480 nm; the ^{1}MLCT absorption moves from 548 to 384 nm; and the highest ^{1}MLCT absorption moves from 376 nm up into the UV region, where it is obscured. The shifts of the lower

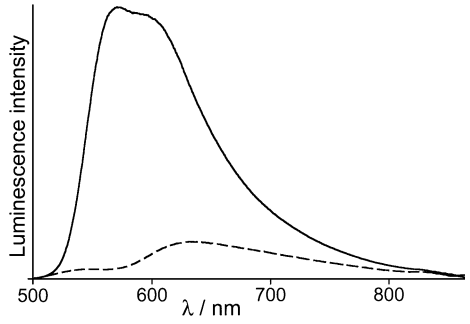

Figure 14. Luminescence spectra of (PPN)$_2$[Os(^{t}Bu$_2$bipy)(CN)$_4$] in a frozen EtOH/MeOH (4:1, v/v) glass at 77 K, in the absence of Zn(ClO$_4$)$_2$·6H$_2$O (dashed line) and in the presence of a large excess of Zn(ClO$_4$)$_2$·6H$_2$O (solid line). The spectra were recorded using excitation with the same optical density in each case, so the intensities are directly comparable.

two bands are both ca. 7000 cm^{-1}, cf. the shifts of 5000 cm^{-1} induced by Ba^{2+} and 4000 cm^{-1} induced by Na^+; there is a clear correlation with the Lewis acidity of the metal ion.

Part (b) of Figure 13 shows the changes in luminescence during the titration of [Os(^{t}Bu$_2$bipy)(CN)$_4$]$^{2-}$ with Zn(ClO$_4$)$_2$ in MeCN. As small amounts of Zn^{2+} (<1 equiv) are added, luminescence appears with a maximum at ca. 750 nm, which rapidly gains in intensity and blue-shifts until it is at 660 nm after the addition of 1 equiv of Zn^{2+}. Thereafter, the changes occur more slowly, and at the end of the titration the luminescence is at 610 nm (cf. 685 nm with Ba^{2+}). Time-resolved measurements show that the luminescence decay profile at the end of the titration fits to three components with lifetimes of ca. 40, 120, and 220 ns, with relative weightings of 6, 61, and 33%, respectively. The reason for such complicated multiexponential behavior has been discussed above: even when the luminescence spectrum shows no further changes, there appears to be a mixture of three (or more) [Os(^{t}Bu$_2$bipy)(CN)$_4$]$^{2-}$/Zn^{2+} aggregates in solution, with the longer two having luminescence lifetimes in the hundreds of nanoseconds region. It is clear that the presence of Zn^{2+} ions has a huge effect on the photophysical properties of [Os(^{t}Bu$_2$bipy)(CN)$_4$]$^{2-}$.

Finally, in this section we note that this metallochromic shift of luminescence also occurs at 77 K in EtOH/MeOH glasses. In the presence of excess Ba(ClO$_4$)$_2$ or Zn(ClO$_4$)$_2$, the emission from [Os(^{t}Bu$_2$bipy)(CN)$_4$]$^{2-}$ is substantially blue-shifted and becomes more intense; for example, in the presence of excess Zn^{2+} at 77 K, the emission from [Os(^{t}Bu$_2$bipy)(CN)$_4$]$^{2-}$ moves from 635 to 575 nm and becomes much more intense (Figure 14).

Electrochemistry. All of the complexes show a reversible one-electron wave corresponding to the Os(II)/Os(III) couple at a modest potential (Table 5), which, however, varies significantly between MeCN and water. For the complexes with bipy, phen, and ^{t}Bu$_2$bipy, the redox couple is at ca. 0 V versus Ag/AgCl in MeCN; for [Os(bpym)(CN)$_4$]$^{2-}$, the Os(II)/Os(III) redox potential is slightly more positive at +0.20 V versus Ag/AgCl, consistent with the fact that bpym is a poorer donor than bipy, so [Os(bpym)(CN)$_4$]$^{2-}$ will have a lower electron density on metal and be harder to oxidize. In water, these are shifted to more positive potentials by ca. 0.5 V, consistent with the reduction in d(π) orbital energies

Table 5. Redox Potentials (V Versus Ag/AgCl) for the Os(II)/Os(III) Couples in Water and MeCN

complex	H_2O[a]	MeCN[b]
$[Os(bipy)(CN)_4]^{2-}$	+0.52	−0.01
$[Os(phen)(CN)_4]^{2-}$	+0.53	0.00
$[Os(bpym)(CN)_4]^{2-}$	+0.66	+0.20
$[Os(^tBu_2bipy)(CN)_4]^{2-}$		−0.05

[a] Base electrolyte, 0.1M KCl. The Na^+ salt of the complex was used. Under these conditions, the $[Fe(CN)_6]^{4-}/[Fe(CN)_6]^{3-}$ redox potential was +0.22 V. [b] Base electrolyte, 0.1M Bu_4NPF_6. The PPN^+ salt of the complex was used. Under these conditions, the ferrocene/ferrocenium redox potential was +0.49 V.

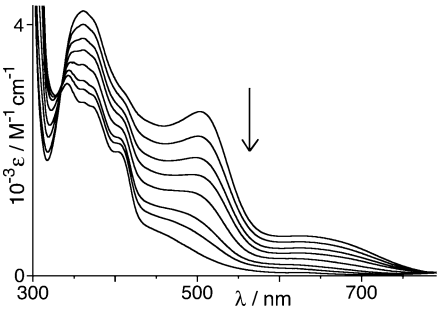

Figure 15. Changes in the electronic spectra of $(PPN)_2[Os(^tBu_2bipy)(CN)_4]$ in MeCN at −20 °C associated with one-electron oxidation of Os(II) to Os(III).

associated with the hydrogen bonding of water molecules to the cyanide ligands.[9] This is similar to what is observed for the analogous Ru(II) complexes,[1,2] although the M(II)/M(III) redox potentials are less positive for M = osmium than for M = ruthenium, in keeping with the general trend for ruthenium and osmium complexes with the same ligand set.

We carried out a UV−vis spectroelectrochemical study of $(PPN)_2[Os(^tBu_2bipy)(CN)_4]$ with an optically transparent thin-layer electrode (OTTLE) cell to see the changes in absorption spectra associated with the Os(II)/Os(III) interconversion in MeCN. The results are in Figure 15. It is clear that the main spectral change in the UV−vis region is a steady decrease in intensity of the three MLCT absorption bands associated with the Os(II) center: the lowest-energy one collapses completely, and the higher-energy two are reduced in intensity and shift slightly to higher energy. This blue shift is consistent with a reduction in energy of the osmium-based d(π) orbitals on oxidation, which will increase the MLCT energy gap, and the reduction in intensity is to be expected as Os(III) must be a poorer π donor than Os(II).

Conclusions

$[Os(bipy)(CN)_4]^{2-}$ and its relatives have a substantial scope for use in supramolecular chemistry, both from the structural and photophysical points of view. The ^{3}MLCT luminescence, although very weak in the native complexes, can be strongly boosted in energy, intensity, and lifetime, in the presence of Lewis-acidic metal cations, which interact with the cyanide groups (metallochromism). This same cyanide/metal cation interaction allows for the ready formation of cyanide-bridged coordination networks with other metal cations (here, Na^+). The photophysical properties of heteronuclear assemblies, in which $[Os(phen)(CN)_4]^{2-}$ chromophores are combined with other luminophores such as Ln(III) cations in the solid state,[6] will be reported in future articles.

Experimental Section

General Details. Organic ligands were purchased from Aldrich and used as received. $Na_4[Os(CN)_6]$ was prepared according to the published method for $K_4[Os(CN)_6]$,[9] but using NaCN instead of KCN. FTIR spectra were recorded on a PerkinElmer Spectrum One instrument with the samples as compressed KBr pellets. UV−vis spectra were recorded on a Cary-50 spectrophotometer; electrospray mass spectra were recorded on a Waters-LCT time-of-flight spectrometer. Cyclic voltammetry measurements were performed in a standard three-electrode cell using platinum-bead working and counter electrodes and a Ag/AgCl reference; ferrocene was used as an internal standard. UV−vis spectroelectrochemical measurements were performed on a Cary-5000 spectrophotometer, using a cooled (−20 °C) OTTLE cell, which has been described previously.[13]

Steady-state emission spectra in the visible region (<800 nm) were measured on PerkinElmer LS-50B or Spex Fluoromax 3 luminescence spectrometers. Steady-state emission spectra in the NIR region (>800 nm), for the measurements of the $[Os(diimine)(CN)_4]^{2-}$ complexes in MeCN (Figure 10), were recorded on a home-built system comprising a cw argon-ion laser (488 nm, power ca. 2 mW at the sample), a Bentham TMC600 spectrograph, and an Andor iDUS CCD camera. The spectrograph and CCD detection system was calibrated with a Bentham CL2 tungsten calibration lamp. In either setup, emission spectra were corrected for the overall system sensitivity at different wavelengths.

Synthesis. The Na^+ salts of the complexes with bipy, phen, and bpym were prepared by the reaction of the appropriate diimine ligand with a slight excess of $Na_4[Os(CN)_6]$, following the published method.[9] At the end of the reaction, solvents were removed, the residue was redissolved in MeOH, and any residual undissolved solid was filtered off. The MeOH soluton was evaporated to dryness, redissolved in the minimum quantity of water, and the crude product was precipitated by the addition of acetone. The complexes were purified by chromatography on Sephadex G10, eluting with water; the main red/brown fraction was collected, and the product was precipitated by the addition of acetone, filtered off, and dried. Yields were typically 70% (based on ligand). Characterization data are as follows.

$Na_2[Os(bpy)(CN)_4]$. IR (KBr pellet): 3502 vs,br, 2092 m, 2052 vs, 2040 vs, 2020 vs, 1636 m, 1463 m, 1443 m, 1419 m, 131 2w, 1276 w, 1245 w, 773 s, 734 w, 563 m, 530 m. Positive-ion ESMS: *m*/*z* 521 $\{Na_3[Os(bpy)(CN)_4]^+\}$, 100%. Negative-ion ESMS: *m*/*z* 425, $[Os(bpy)(CN)_3]^-$, 60%; 453, $[Os(bpy)(CN)_4H]^-$, 100%; 475, $\{Na[Os(bpy)(CN)_4]\}^-$, 70%. Anal. Found: C, 27.1; H, 2.9; N, 13.6. Calcd for $Na_2[Os(bpy)(CN)_4]\cdot 6H_2O$: C, 27.8; H, 3.3; N, 13.9.

$Na_2[Os(phen)(CN)_4]$. IR (KBr pellet): 3428 vs,br, 2090 m, 2042 vs, 2019 sh, 1631 m, 1427 s, 1407 sh, 1355 w, 845 m, 782 m, 723 m, 604 m, 551 m, 530 m. Positive-ion ESMS: *m*/*z* 545, $\{Na_3[Os(phen)(CN)_4]\}^+$, 100%. Negative-ion ESMS: *m*/*z* 477, $[Os(phen)(CN)_4H]^-$, 100%; 499 $\{Na[Os(phen)(CN)_4]\}^-$, 10%. Anal. Found: C, 30.1; H, 2.8; N, 13.5. Calcd for $Na_2[Os(phen)(CN)_4]\cdot 6H_2O$: C, 28.9; H, 3.1; N, 14.3.

$Na_2[Os(bpym)(CN)_4]\cdot 4H_2O$. IR (KBr pellet): 3596 sh, 3435 vs,br, 2100 m, 2062 sh, 2046 vs, 202 9sh, 1631 w, 1400 s, 1181 w, 1025 w, 837 w, 752 w, 530 w. Positive-ion ESMS: *m*/*z* 523, $\{Na_3[Os(bpym)(CN)_4]\}^+$, 100%. Negative-ion ESMS: *m*/*z* 428,

(13) Lee, S.-M.; Kowallick, R.; Marcaccio, M.; McCleverty, J. A.; Ward, M. D. *J. Chem. Soc., Dalton Trans.* **1998**, 3443.

[Os(bpym)(CN)$_3$]}, 10%; 454, [Os(bpym)(CN)$_4$]}, 30%; 477, {Na[Os(bpym)(CN)$_4$]}$^-$, 20%. Anal. Found: C, 24.4; H, 2.2; N, 18.7. Calcd for Na_2[Os(bpym)(CN)$_4$]·5H_2O: C, 24.5; H, 2.7; N, 19.0.

The above Na^+ salts were converted to their organic-soluble $(PPN)^+$ salts by adding a concentrated aqueous solution of the Na^+ salt to a warm aqueous solution containing an excess of PPNCl, according to the method of Evju and Mann.[14] The resulting precipitates were filtered off, dried, and recrystallized by diffusion of hexane vapor into an acetone solution of the complex. The cation metatheses gave yields of 70−90% yields of the $(PPN)^+$ salts. Characterization data are as follows.

$(PPN)_2$[Os(bpy)(CN)$_4$]. IR (KBr pellet): 3412 br,vs, 2090 m, 2038 s, 2026 sh, 1637 m, 1619 sh, 1588 sh, 1482 w, 1467 w, 1438 m, 1384 w, 1297 sh, 1261 s, 1116 s, 1025 w, 998 w, 802 w, 769 sh, 724 s, 695 s, 550 s, 532 s, 499 m. Positive-ion ESMS: *m*/*z* 538, $(PPN)^+$, 100%. Negative-ion ESMS: *m*/*z* 425, [Os(bpy)(CN)$_3$]$^-$, 100%; 989, {(PPN)[Os(bpy)(CN)$_4$]}$^-$, 10%. Anal. Found: C, 62.6; H, 5.0; N, 6.6. Calcd for $(PPN)_2$[Os(bpy)(CN)$_4$]·5.5H_2O: C, 63.5; H, 4.9; N, 6.9.

$(PPN)_2$[Os(phen)(CN)$_4$]. IR (KBr pellet): 3405 br,vs, 3077 w, 3058 w, 2091 m, 2044 vs, 2025 sh, 1707 m, 1635 m, 1587 m, 1482 m, 1438 s, 1407 w, 1384 w, 1297 sh, 1262 vs, 1180 sh, 1116 vs, 1025 w, 998 m, 845 m, 802 m, 754 sh, 747 m, 723 vs, 696 vs, 551 vs, 532 vs, 499 s. Positive-ion ESMS: *m*/*z* 538, $(PPN)^+$, 100%. Negative-ion ESMS: *m*/*z* 476, [Os(phen)(CN)$_4$H]$^-$, (100%). Anal. Found: 66.1; H, 4.6; N, 6.6. Calcd for $(PPN)_2$[Os(phen)(CN)$_4$]·2H_2O·(acetone): 66.4; H, 4. 8; N, 6.8.

$(PPN)_2$[Os(bpm)(CN)$_4$]. IR (KBr pellet): 3413 br,vs, 2100 m, 2061 s, 2030 s, 1637 m, 1618 m, 1588 sh, 1482 w, 1437 m, 1397 m, 1384 sh, 1296 sh, 1260 s, 1221 sh, 1185 w, 1116 s, 1025 w, 998 w, 750 m, 724 s, 693 s, 550 m, 532 s, 500 m. Positive-ion ESMS: *m*/*z* 538, $(PPN)^+$, 100%. Negative-ion ESMS: *m*/*z* 454, [Os(bpm)(CN)$_3$]$^-$, 100%; 992 {(PPN)[Os(bpm)(CN)$_4$]}$^-$, 10%. Anal. Found: C, 59.2; H, 5.0, N, 8.1. Calcd for $(PPN)_2$[Os(bpm)-(CN)$_4$]·10H_2O: C, 59.0; H, 5.1; N, 8.2.

$(PPN)_2$[Os(^{t}Bu$_2$bipy)(CN)$_4$]. IR (KBr pellet): 3409 vs,br, 3077 w, 2956 m, 2090 m, 2047 vs, 2038 sh, 1632 m, 1588 sh, 1482 m, 1438 s, 1410 w, 1384 w, 1364 w, 1297 sh, 1259 vs, 1180 w, 1116 vs, 1025 w, 997 m, 852 w, 801 w, 747 m, 724 vs, 695 s, 552 s, 532 vs, 498 s. Positive-ion ESMS: *m*/*z* 538, $(PPN)^+$, 100%. Negative-ion ESMS: *m*/*z* 564, [Os(^{t}Bu$_2$bipy)(CN)$_4$H]$^-$, 100%; 1102, {(PPN)[Os(^{t}Bu$_2$bipy)(CN)$_4$]}$^-$, 2%. Anal. Found: C, 65.6; H, 5.4, N, 6.4. Calcd for $(PPN)_2$[Os(^{t}Bu$_2$bipy)(CN)$_4$]·4H_2O: C, 66.0; H, 5.4; N, 6.6.

X-ray Crystallography. X-ray quality crystals of Na_2[Os(bipy)-(CN)$_4$]·4H_2O, Na_2[Os(phen)(CN)$_4$]·5H_2O, Na_2[Os(bpym)(CN)$_4$]·4H_2O, and Na_2[Os(bpym)(CN)$_4$]·8H_2O were grown by the slow evaporation of aqueous solutions of the complexes. Crystals of $(PPN)_2$[Os(^{t}Bu$_2$bipy)(CN)$_4$]·2H_2O·(Me_2CO) were grown by diffusion of hexane vapor into a solution of the complex in acetone.

In all of the cases, a suitable crystal was mounted on a Bruker APEX-2 diffractometer equipped with graphite-monochromatized Mo Kα radiation. Details of selected structural parameters are collected in Tables 1; details of the crystal, data collection, and refinement parameters are in Table 2. After integration of the raw data and merging of equivalent reflections, an empirical absorption correction was applied based on the comparison of multiple symmetry-equivalent measurements.[15] The structures were solved by direct methods and refined by full-matrix least-squares on weighted F^2 values for all of the reflections using the *SHELX* suite of programs.[16] None of the refinements presented any significant problems. For coordinated and lattice water molecules, hydrogen atoms were added only when both of them showed up clearly in a refinement using only low-angle data; they were then fixed in position with O−H distances of 0.85 Å. In all of the cases, there are numerous lattice water molecules, which were refined with either 50 or 100% site occupancy, as required to generate reasonable thermal displacement parameters.

Acknowledgment. We thank the European Commission for a Marie-Curie postdoctoral fellowship to S.G.B. (contract M1F1-CT-2005-513860). We also thank Prof. Chris Hunter for assistance with fitting the luminescence titrations and Dr. Jim Reid and Dr. Julia Weinstein for access to luminescence equipment (which was purchased in part by an equipment grant from the Royal Society).

Supporting Information Available: CIF files of crystal structures. This material is available free of charge via the Internet at http://pubs.acs.org.

IC701169C

(14) Evju, J. K.; Mann, K. R. *Chem. Mater.* **1999**, *11*, 1425.

(15) Sheldrick, G. M. *SADABS*: *A Program for Absorption Correction with the Siemens SMART System*; University of Göttingen: Göttingen, Germany, 1996.

(16) *SHELXTL Program System Version 5.1*; Bruker Analytical X-ray Instruments Inc.: Madison, WI, 1998.